Biochimica et Biophysica Acta, 778 (1984) 570–578
Elsevier

BBA 72387

DIELECTRIC ANALYSIS OF MITOCHONDRIA ISOLATED FROM RAT LIVER

II. INTACT MITOCHONDRIA AS SIMULATED BY A DOUBLE-SHELL MODEL *

KOJI ASAMI and AKIHIKO IRIMAJIRI

Department of Physiology, Kochi Medical School, Nankoku, Kochi 781-51 (Japan)

(Received June 20th, 1984)

Key words: Dieletric dispersion; Mitochondrion; Outer membrane; Inner membrane; Intramitochondrial compartment; Membrane capacity; Permittivity; Conductivity; Double-shell model

The dielectric dispersion of isolated intact mitochondria in suspension has been measured between 10 kHz and 500 MHz. In isotonic KCl media at 4°C, the mitochondria maintained their characteristic 'double membrane' structure as examined by electron microscopy, and the observed dispersion curves were successfully simulated in terms of a superposition of two sub-dispersions having different characteristic frequencies and different permittivity magnitudes. Taking these observations into account we analyzed the dispersion data on the basis of a 'double-shell' model in which two concentric shells are meant to represent the mitochondrial outer and inner membranes. The analyses by a computerized curve-fitting method revealed that: (i) electric capacities for the outer and the inner membrane are 1.7 and 0.5 $\mu F/cm^2$, respectively, (ii) relative permittivity for the inner compartment (or the equivalent homogeneous matrical space) = 50–60, (iii) outer compartment-to-external conductivity ratio = 0.4–0.6, and (iv) inner compartment-to-external conductivity ratio = 0.14. The implications of these parameter values are discussed with due attention paid to the limitations inherent in our 'double-shell' model approach.

Introduction

The preceding paper by Asami et al. [1] (hereafter, Paper I), dealing with a dielectric dispersion analysis on the suspension of mitoplasts, has presented a plausible set of electrical parameters that are related to the intramitochondrial structure. The probing tool there employed was a conventional 'single-shell' model consisting of only two phases, viz., one limiting membrane and one homogeneous, internal compartment enclosed therewith (Fig. 1a).

In the analysis of intact mitochondria, however, the single-shell model appears to be of limited

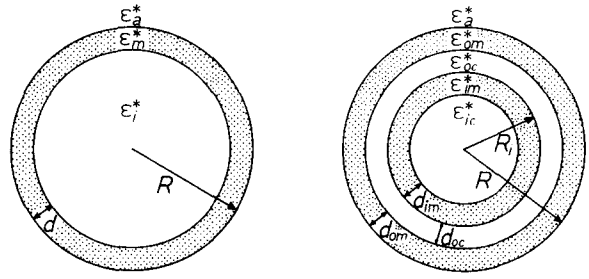

(a) SINGLE-SHELL (b) DOUBLE-SHELL

Fig. 1. Dielectric models for an intact mitochondrion: (a) Single-shell model, (b) Double-shell model. Complex relative permittivity (ϵ_x^*) for each phase is defined as $\epsilon_x^* = \epsilon_x - j\kappa_x/2\pi f\epsilon_v$ where ϵ = relative permittivity, κ = conductivity, $j = (-1)^{1/2}$, f = frequency, and ϵ_v = permittivity of vacuum. Subscripts (x's) have the following meanings: a, suspending medium; m, membrane; i, internal compartment ('matrix'); om, outer membrane; im, inner membrane; oc, outer compartment ('intermembrane space'); and ic, inner compartment ('matrix').

* For Paper I see Ref. 1.

value because, in this case, at least four discrete phases are involved in the ultrastructure of particles [2]. These include, to name from surface to core, the outer membrane, intermembrane space, inner membrane, and matrix. Therefore the next step towards a more elaborate analysis would be to adopt a 'double-shell' model (Fig. 1b) as the exploring framework for simulation. A successful application of this model to the bio-dielectric work has already been reported by Irimajiri et al. [3] who dealt with cultured lymphoma cells.

The present paper describes how to simulate the dielectric behavior of isolated intact mitochondria in suspension and what meanings then the analyzed phase parameters have to our understanding of the mitochondrial organization.

Theoretical

The models and relevant symbols used are depicted in Fig. 1. Theoretical expression for the single-shell model that has been employed in Paper I is as follows: ϵ^*, the equivalent homogeneous complex permittivity of a suspension of volume fraction ϕ is given by

$$\left(\frac{\epsilon^* - \bar{\epsilon}_p^*}{\epsilon_a^* - \bar{\epsilon}_p^*}\right)\left(\frac{\epsilon_a^*}{\epsilon^*}\right)^{1/3} = 1 - \phi \tag{1}$$

where

$$\bar{\epsilon}_p^* = \epsilon_m^* \frac{2(1-v)+(1+2v)E}{(2+v)+(1-v)E} \tag{2}$$

with $v = (1 - d/R)^3$ and $E = \epsilon_i^*/\epsilon_m^*$.

For the double-shell model (Fig. 1b), on the other hand, the interim parameter, $\bar{\epsilon}_p^*$, should be modified so as to properly represent the internal concentric structure of the particle. As already developed by Irimajiri et al. [4] on the basis of Maxwell [5], $\bar{\epsilon}_p^*$ for the stratified sphere may be written

$$\bar{\epsilon}_p^* = \epsilon_{om}^* \frac{2(1-v_1)+(1+2v_1)E_1}{(2+v_1)+(1-v_1)E_1} \tag{3}$$

where $v_1 = (1 - d_{om}/R)^3$ and $E_1 = \bar{\epsilon}_{oc}^*/\epsilon_{om}^*$. Here, $\bar{\epsilon}_{oc}^*$ has been introduced to represent the spherical region of radius $(R - d_{om})$ and may be analogously expressed as

$$\bar{\epsilon}_{oc}^* = \epsilon_{oc}^* \frac{2(1-v_2)+(1+2v_2)E_2}{(2+v_2)+(1-v_2)E_2} \tag{4}$$

where $v_2 = (1 + d_{oc}/R_i)^{-3}$ and $E_2 = \bar{\epsilon}_{im}^*/\epsilon_{oc}^*$. Finally, $\bar{\epsilon}_{im}^*$ may be given by

$$\bar{\epsilon}_{im}^* = \epsilon_{im}^* \frac{2(1-v_3)+(1+2v_3)E_3}{(2+v_3)+(1-v_3)E_3} \tag{5}$$

where $v_3 = (1 - d_{im}/R_i)^3$ and $E_3 = \epsilon_{ic}^*/\epsilon_{im}^*$. Thus, combination of Eqn. 1 with Eqns. 3–5 enables calculation of ϵ^* when a set of morphometric and electrical phase parameters of the double-shell model is provided.

To grasp the general features of the dielectric behavior predictable from the model we calculated ϵ^* for a hypothetical suspension ($\phi = 0.3$) of the double-shells having the parameters as defined in legend to Fig. 2, in which only the inter-shell distance, d_{oc}, was varied from zero to the full radius. The results (Fig. 2) are expressed as frequency dependence curves for relative permittivity (ϵ) and conductivity (κ) which are related to ϵ^* through

$$\epsilon^* = \epsilon + \kappa/j(2\pi f)\epsilon_v \tag{6}$$

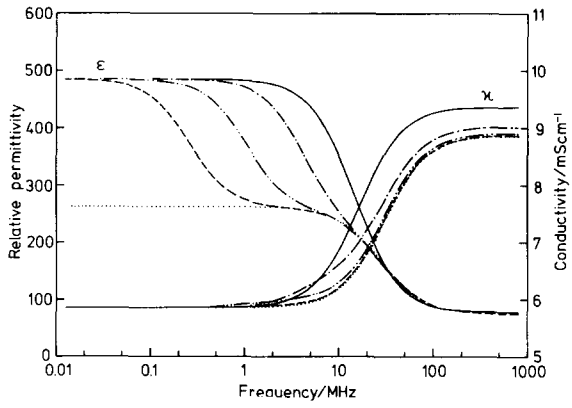

Fig. 2. Theoretical frequency dependence of relative permittivity (ϵ) and conductivity (κ), predictable from the single-shell model (solid lines) or the double-shell model (interrupted lines). Calculations employ the following parameters: $\epsilon_a = \epsilon_{oc} = \epsilon_{ic} = \epsilon_i = 80$, $\kappa_a = \kappa_{oc} = \kappa_{ic} = \kappa_i = 10$ mS/cm, $\epsilon_m = \epsilon_{om} = \epsilon_{im} = 10$, $\kappa_m = \kappa_{om} = \kappa_{im} = \kappa_a \cdot 10^{-6}$, $\phi = 0.30$, $R = 0.5$ μm, $d = d_{om} = d_{im} = 7.0$ nm; and d_{oc} in nm is varied as: 0 (·····), 5 (------), 20 (-·-·-·-), and 80 (-·-·-); and $R_i = 0$ (————).

As illustrated, the double-shell model gave rise to at least two dispersions whose separation in the log frequency axis was a decreasing function of d_{oc}. In the extreme cases where $R_i = 0$ and $d_{oc} = 0$ the dispersion curves reduced to those of the single-shell model.

Methods

Rat liver mitochondria were prepared by a sucrose step gradient method described in Paper I. After pelleted by centrifugation in a washing solution containing 0.25 M sucrose and 5 mM Tris-HCl (pH 7.4), the isolated intact mitochondria were divided into two aliquots each of which was resuspended and equilibrated in the test medium at 4°C for at least 1 h. Two test media, A and B, with differing salt concentrations but with the same osmolality (280 mosmol/kg H_2O) and pH (adjusted to 7.4 with 10 mM Tris-HCl) were used: Medium A contained 130 mM KCl plus 15 mM sucrose and Medium B, 65 mM KCl plus 125 mM sucrose. The final wash with the test media was made immediately before dielectric measurements and the supernatants from this step were subjected to the determination of ϵ_a and κ_a.

Dielectric measurements, electron microscopic morphometry and protein assay were performed exactly as described in Paper I.

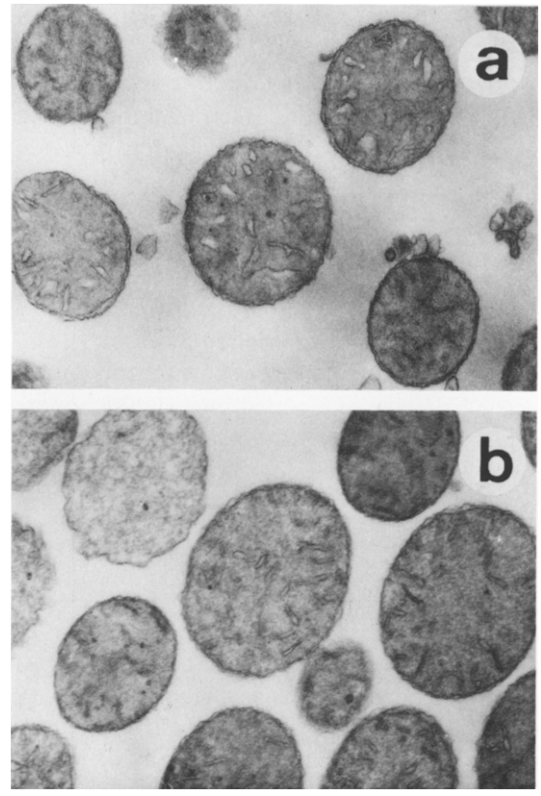

Fig. 3. Electron micrographs of isolated intact mitochondria incubated in medium A at: (a) 4°C and (b) 25°C. Magnification, 20000×.

Results

Morphology

Electron microscopic observations (Fig. 3) revealed that transfer of the specimen from the initial sucrose medium to an isotonic KCl medium (Medium A) elicited a structural change in the isolated mitochondria from the 'condensed' to the 'orthodox' form during incubation for 1 h. However, the preservation of the outer membranes was temperature dependent; i.e., at 4°C the double membranes structure characteristic of the intact mitochondria was well preserved (Fig. 3a), while at 25°C a frequent detachment of the outer membranes ('mitoplasts') and a greater degree of particulate swelling were both observed (Fig. 3b). Therefore, the condition for equilibration with the test media was chosen at 4°C at which temperature the occurrence of damaged mitochondria was less than 4%. Subsequent dielectric measurements and morphometric analyses were made at this same temperature throughout. The stereologically corrected mean radius was found to be 0.46 μm for the mitochondria equilibrated in meidum A or B followed by fixation at 4°C. The quantitative assessment of the intermembrane space, d_{oc}, was by no means feasible because of the irregular spacing between the two membranes as apparent from Fig. 3. Therefore, a rough estimate of 30 nm was taken for d_{oc} together with an estimate for d_{om} and d_{im} of 7 nm; these figures were used in the analyses described below.

Dielectric dispersion curve and phenomenological analysis

A typical example of measurements on the intact mitochondria is shown in Fig. 4a. The steep rise of permittivity as frequency decreased, espe-

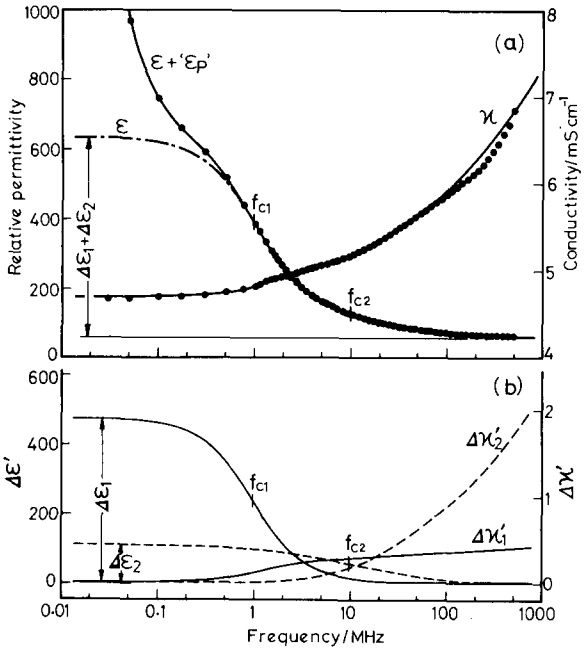

Fig. 4. Dielectric dispersion curves for intact mitochondria suspended in medium A at 4°C. (a) Filled circles, observed. Solid lines depict the best-fit simulation based on combination of Eqns. 7 and 8. 'ϵ_P' refers to arfefactual components due to electrode polarization capacitances. Dot and dash line, ϵ-curve corrected for 'ϵ_P'. (b) Solid lines, lower-frequency dispersion characterized by permittivity increment $\Delta\epsilon_1$ and characteristic frequency f_{c1}. Broken lines, higher-frequency dispersion characterized by permittivity increment $\Delta\epsilon_2$ and characteristic frequency f_{c2}. $\Delta\epsilon'$ and $\Delta\kappa'$ are interrelated according to Eqn. 9.

cially in the region below 1 MHz, was due to the electrode polarization capacitances C_P superposed on ϵ for the suspension. To correct for this effect we applied the following formula [6]:

$$C_P/C_1 = \epsilon_P = Af^{-m} \tag{7}$$

where f is frequency in MHz; C_1 ('cell constant'), A and m are constants determined experimentally. The result of such corrections, with $A = 3.87$ and $m = 1.50$, of the low-frequency data is indicated by the dash and dot line in Fig. 4a.

The next trial made was to simulate the corrected data points in terms of two Cole-Cole type [7] dispersions formulated by

$$\epsilon^* = \epsilon_h + \frac{\Delta\epsilon_1}{1+(jf/f_{c1})^{\beta_1}} + \frac{\Delta\epsilon_2}{1+(jf/f_{c2})^{\beta_2}} + \frac{\kappa_1}{j(2\pi f)\epsilon_v} \tag{8}$$

Here, $\Delta\epsilon$'s are permittivity increments, f_c's characteristic frequencies, β's the Cole-Cole parameters, j is unit imaginary, numerical subscripts denote dispersions 1 and 2; and subscripts 1 and h refer to the limiting low- and high-frequency values, respectively. Curve fitting based on Eqn. 8 were carried out by a nonlinear least-squares minimization algorithm to yield the best-fit parameters (Table I) and the resulting curves for both ϵ and κ (Fig. 4a). The fitting as a whole was more than satisfactory. Thus, the two dispersions were successfully separated as depicted in Fig. 4b. It is to be noted that the conductivity curves, denoted by $\Delta\kappa_1'$ and $\Delta\kappa_2'$ (where $\kappa = \kappa_1 + \Delta\kappa_1' + \Delta\kappa_2'$), are the results of computation assuming a relation of the form (cf. Appendix B to Paper I):

$$\left.\begin{aligned} \Delta\kappa' &= 2\pi f\epsilon_v\Delta\epsilon'' \\ \Delta\epsilon' - j\Delta\epsilon'' &= \frac{\Delta\epsilon}{1+(jf/f_c)^{\beta}} \end{aligned}\right\} \tag{9}$$

which implies, as discussed in Paper I, that, if $\beta \neq 1$, neither the curves for $\Delta\kappa_1'$ and $\Delta\kappa_2'$ in Fig. 4b nor the resultant κ in Fig. 4a should level off in the frequency domain.

Fig. 5 shows the complex plane plots of data in Fig. 4. Apparently, the trace in the permittivity plane (Fig. 5a) is asymmetric with respect to the

TABLE 1

PHENOMENOLOGICAL DIELECTRIC PARAMETERS OBTAINED FROM CURVE FITTING

Data are same as in Figs. 4 and 5.

κ_1 (mS/cm)	ϵ_h	Dispersion 1			Dispersion 2		
		$\Delta\epsilon_1$	f_{c1} (MHz)	β_1	$\Delta\epsilon_2$	f_{c2} (MHz)	β_2
4.70	58.2	469	0.957	0.916	108	9.89	0.676

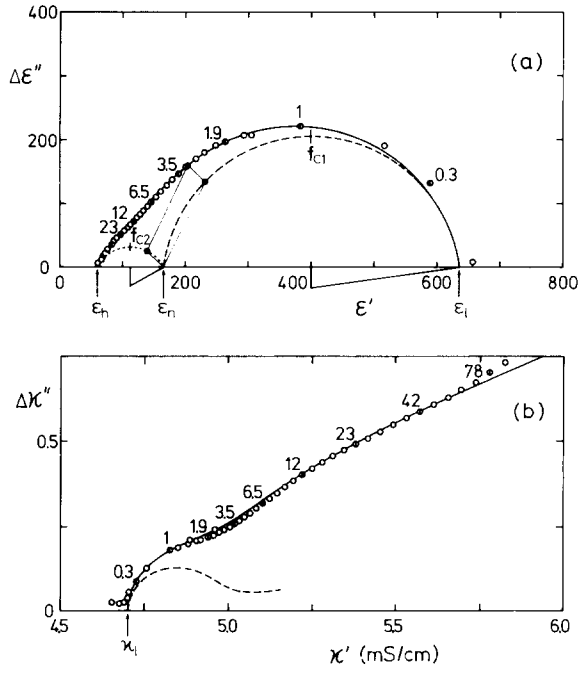

Fig. 5. Complex permittivity (a) and conductivity (b) plane plots of data in Fig. 4. Solid lines depict the best-fit curves obtained by a vectorial synthesis of two subdispersions (broken lines) of a Cole-Cole type. f_{c1} and f_{c2} are the respective characteristic frequencies. Number on each point refers to marker frequency in MHz. Filled circles in parallelogram in (a) correspond to 3 MHz.

half-value frequency at which $\epsilon = \epsilon_h + \Delta\epsilon/2$. The same is true for the conductivity plots (Fig. 5b). Here again, however, an excellent fitting between theory and experiment has anyway been realized. The uniqueness in separating those two sub-dispersions from the measured is clearly shown by the built-up parallelogram connecting the common frequency points (in this case, 3 MHz) in Fig. 5a.

Determination of phase parameters by the shell models

In Fig. 2 we have already examined the behavior of the double-shell model by applying the parameter values taken as being relevant to the intact mitochondria. The calculation gave a family of dispersion curves each of which was a composite of two distinct dispersions. On the other hand, the observed dispersions were also of a similar, composite type as just described. The main difference between the two was such that the sub-dispersions involved in the latter were generally of a Cole-Cole type while those predicted from the model were of a Debye type when $\phi < 0.3$; in other words, we formally have

$$\beta_1 < 1 \text{ and } \beta_2 < 1 \text{ (for the observed)} \quad (10)$$

and

$$\beta_1 = \beta_2 = 1 \text{ (for the predicted)} \quad (11)$$

Strictly speaking, therefore, the use of the double-shell model as it is should place limitations upon the simulation of the observed dispersion curves. While keeping this in mind, we have attempted to curve-fit on the basis of the double-shell model with a typical result such as illustrated in Fig. 6. Here, the fitting of curve a was performed under the restrictions that the values of the dielectric parameters (i.e., $\Delta\epsilon_1$, f_{c1}, $\Delta\epsilon_2$, f_{c2} and ϵ_h) to be predicted were fixed to those read from the Cole-Cole plots, viz., the values listed in Table I. Curve b stands for the nonlinear least-squares fitting conducted without the above restrictions except for ϵ_1 whose level was fixed at 635 ($= \Delta\epsilon_1 + \Delta\epsilon_2 + \epsilon_h$) which was the same as for curve a. Curve c represents the best fitting with the single-shell model. Values of the phase parameters thus determined are given in Table II. As clearly shown, the 'double-shell model' approach such as represented by curve b gave the most satisfactory fitting. Accordingly, our routine analysis employed

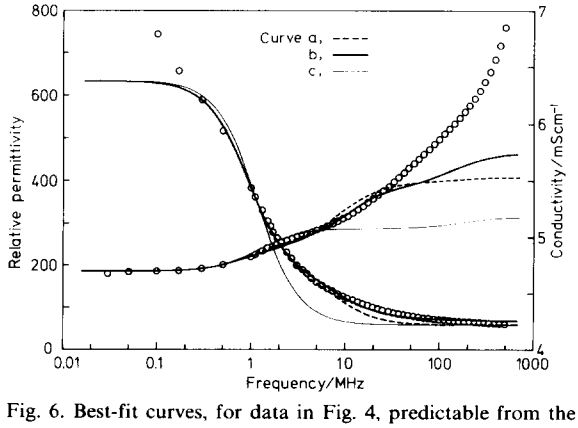

Fig. 6. Best-fit curves, for data in Fig. 4, predictable from the double-shell model (————, ------) or the single-shell model (————). Calculations employ three sets of phase parameters listed in Table II. Open circles, observed.

TABLE II

PHASE PARAMETERS OBTAINED FROM CURVE FITTINGS ILLUSTRATED IN Fig. 6

Assumed parameters: $\kappa_{om} = \kappa_{im} \leqq \kappa_a \cdot 10^{-6}$, $\epsilon_{oc} = \epsilon_a$, $d_{om} = d_{im} = 7.0$ nm, $d_{oc} = 30$ nm. Determined parameters: $\kappa_a = 9.50$ mS/cm, $\epsilon_a = 87.7$, $R_o = 0.460$ μm, $\phi = 0.374$. These values are fixed throughout.

Curve	Model	Phase parameters				
		ϵ_{om}	ϵ_{im}	ϵ_{ic}	κ_{oc} (mS/cm)	κ_{ic} (mS/cm)
a	Double-shell	12.1	3.1	14	4.1	0.86
b	Double-shell	12.1	3.4	54	4.0	1.21
		ϵ_m		ϵ_i	κ_i (mS/cm)	
c	Single-shell	12.1		23	0.56	

TABLE III

PHASE PARAMETERS FOR INTACT MITOCHONDRIA IN MEDIA A AND B AT 4°C

Values are expressed as the mean (range of scatter) of 4 (for medium A) or 3 (for medium B) separate determinations for each medium. Analyses were preformed on the following assumptions: $k_{om} = \kappa_{im} \leqq \kappa_a \cdot 10^{-6}$, $\epsilon_{oc} = \epsilon_{oc} = \epsilon_a$, $d_{om} = d_{im} = 7.0$ nm, $d_{oc} = 30$ nm, and $R_o = 0.460$ μm.

Medium		A	B	A/B [a]
KCl	(mM)	130	65	2.0
ϵ_a		86.9	87.7	0.99
κ_a	(mS/cm)	9.49	4.78	2.0
ϵ_{om}		13.3 (11.1–15.6)	14.0 (11.6–16.2)	0.95
ϵ_{im}		3.8 (3.1–4.5)	4.3 (3.1–5.7)	0.89
κ_{oc}	(mS/cm)	3.8 (2.7–4.5)	2.9 (2.8–3.0)	1.3
κ_{ic}	(mS/cm)	1.2 (1.1–1.3)	0.71 (0.66–0.74)	1.7
ϵ_{ic}		58 (52–70)	46 (43–50)	1.3
C_{om}	(μF/cm^2)	1.69 (1.40–1.97)	1.78 (1.46–2.05)	0.95
C_{im}	(μF/cm^2)	0.48 (0.40–0.57)	0.54 (0.40–0.73)	0.89
κ_{oc}/κ_a		0.40 (0.29–0.47)	0.61 (0.60–0.63)	0.66
κ_{ic}/κ_a		0.13 (0.12–0.14)	0.15 (0.14–0.16)	0.87
v [b]	(μl/mg protein)	2.8 (2.5–3.1)	2.6 (2.4–2.9)	1.1

[a] Ratio of value for medium A to value for medium B.

[b] Specific volume.

this same method; the numerical results obtained with the mitochondria incubated in media A and B are summarized in Table III. Data for the specific volume (v) are also attached.

Table III shows that the two-fold difference in the medium ionic strengths as reflected by κ_a influenced only slightly the membrane-related parameters, ϵ_{om} and ϵ_{im} (hence, C_{om} and C_{im}), moderately both κ_{oc} and ϵ_{ic}, and rather severely the core conductivity κ_{ic}.

Discussion

Double-shell model as the probing tool

The general theory of the multiple-stratified shell model [4] predicates that the system gives rise to multiple dielectric dispersions, the number of which corresponds to the number of interfaces lying between the successive shell phases. For the 'double-shell' structure, therefore, the full number of such sub-dispersions should be four because

every shell is demarcated by two boundaries. However, under the present conditions of the mitochondrial dimension (membrane thickness/particulate diameter ratio $\approx 10^{-2}$) and of the electrical parameters (membrane/aqueous phase conductivity ratio $\leq 10^{-6}$), only two out of four sub-dispersions have predominated, as seen in the model calculation (Fig. 2) and also in the simulation of the observed behavior (Fig. 6, curve b). Such being the case, our analysis relied upon the double-shell model while neglecting, to a first approximation, the possible involvement of distributed size and phase parameter values. In practice of the curve fittings, we took full advantage of the model's characteristic behavior that can be disclosed by a perturbation method (cf. Appendix) similar to one already devised by Hanai et al. [8]. The single-shell model has been proved to be a poor model for the present specimen (Fig. 6, curve c).

Validity of the assumptions employed

Our analysis presented above has been based on the following assumptions: (1) $\kappa_{om}/\kappa_a = \kappa_{im}/\kappa_a \leq 10^{-6}$, (2) $\epsilon_{oc} = \epsilon_a$, (3) $d_{oc} = 30$ nm, and (4) $d_{om} = d_{im} = 7$ nm. Among these, assumption 1 ($\kappa_{om} \simeq 0$) was essential since, without this restraint, an accurate determination of ϕ, the volume concentration of a given suspension, would not have been feasible. Although the practically 'null' conductivity of the membrane phase appears valid for most biological membranes including the mitochondrial, we dare to question what difference should emerge in the analyzed parameters if the outer and inner membranes are more conductive than here assumed. The answer is, as shown in Table IV, that as far as the mitochondrial membranes of κ_m's $\leq 10^{-5} \times \kappa_a$ are concerned the errors in the analysis due to a misestimate for κ_m values as being one order of magnitude less conductive than the real ones are at most 2-3%. The κ_m-value of $10^{-5} \times \kappa_a$ corresponds to a membrane resistance of approx. 10 $\Omega \cdot cm^2$, too small a value for the natural membranes. If, however, the outer membrane resistivity is actually as low as approx. 1 $\Omega \cdot cm^2$ or less, then the present analysis using the assumption, κ_m's $\leq 10^{-6} \times \kappa_a$, would lose ground especially for the determinations of ϵ_{om} and κ_{oc}, as clear from Table IV. The other parameters are nonetheless relatively tough to such a loose assumption for κ_m values.

Assumption 2 ($\epsilon_{oc} = \epsilon_a$) has been introduced rather arbitrarily but inevitably because the response of the pertinent dispersion curves was exceedingly dull to changes in ϵ_{oc} (see Appendix,

TABLE IV

EFFECT OF MEMBRANE CONDUCTIVITIES ON THE ANALYSIS OF PHASE PARAMETERS

Curve-fitting analysis is made for different values of κ_{om} or κ_{im}. Data are from Fig. 4. Values in (A) refer to the reference state obtained with $\kappa_{om} = \kappa_{im} = 0$. Calculations in (B) and (C) are made with $\kappa_{im} = 0$ and $\kappa_{om} = 0$, respectively; and the results are expressed as '% deviation' from (A). C_{om} and C_{im}, derived respectively from ϵ_{om} and ϵ_{im}.

	ϕ	Phase parameter					Membrane capacity	
		ϵ_{om}	ϵ_{im}	ϵ_{ic}	κ_{oc} (mS/cm)	κ_{ic} (mS/cm)	C_{om} (μF/cm^2)	C_{im} (μF/cm^2)
(A)	0.374	12.1	3.35	54.1	3.98	1.21	1.53	0.42
		(%)						
(B) κ_{om}/κ_a [a]								
10^{-5}	+0.1	+2.4	−0.3	−0.0	+0.6	+0.2	1.56	0.42
10^{-4}	+1.0	+23	−2.5	−0.4	+6.0	+1.3	1.88	0.41
10^{-3}	+5.2	+214	−7.0	−1.4	+48	+5.7	4.80	0.39
(C) κ_{im}/κ_a [a]								
10^{-5}	0	0	+1.0	−0.2	−1.0	+0.2	1.53	0.43
10^{-4}	0	0	+9.6	−2.3	−9.5	+2.6	1.53	0.46
10^{-3}	0	0	+93	−12	−71	+28	1.53	0.82

[a] $\kappa_a = 9.496$ mS/cm.

Table A1). This stems from the fact that the relative volume occupied by the outer compartment (i.e., intermembrane space) is only approx. 18% when calculated using the morphometric parameters: $R = 460$ nm, $d_{om} = 7$ nm, and $d_{oc} = 30$ nm. Consequently, our analysis is ineffectual with respect to the determination of ϵ_{oc}.

The intermembrane distance ($d_{oc} = 30$ nm) and the membrane thicknesses ($d_{om} = d_{im} = 7$ nm) have not been simply assumed but rather more experimentally based as compared with the other fixed parameters. However, we still call them 'assumption' since the electron microscopic images of membrane-related fine structures were variable depending on the fixation methods employed and hence did not necessarily reflect the true thickness of the membranes. What uncertainty then should arise to affect the final results of analysis? Numerical assessment revealed that (1) the best-fit value of κ_{oc} changes with change in d_{oc} such that the product $\kappa_{oc} d_{oc}$ is kept relatively constant and (2) the membrane permittivities, ϵ_{om} and ϵ_{im}, are to be analyzed as being proportional to the respective membrane thicknesses, d_{om} and d_{im}. Therefore, ambiguity in d_{oc} even fatally affected the determinations of κ_{oc}, whereas the problem arising from uncertainty in d_{om} or d_{im} could be circumvented [9] by taking membrane capacitance C_m instead of the membrane permittivity ϵ_m which is related to C_m through

$$C_m = \epsilon_v \epsilon_m / d_m \tag{12}$$

where $\epsilon_v = 8.854 \cdot 10^{-8}$ μF/cm (permittivity of vacuum).

Evaluation of the analyzed phase parameters

The result of analysis concerning C_{om} and C_{im} (Table III) appears satisfactory to the point that either parameter falls within 0.5–2 μF/cm^2, a range that has been widely accepted for the biomembrane capacitances [10]. To be meticulous, however, there is an approx. 3-fold difference between C_{om} and C_{im}, the reason for which is at present not obvious. Possible misestimates for d_m values have nothing to do with this matter, as noted in the preceding section. Nor critical is a moderate misestimate for R_i, the radius of spherical region covered with the inner membrane. One possible mechanism is that different degrees to which the two membranes wrinkle or infold may well change the effective membrane area which is difficult to measure with accuracy but does affect the analyzed values of C_m expressed in μF/cm^2. This mechanism might be responsible, at least in part, for the difference between the present C_{im}-value of approx. 0.5 μF/cm^2 and the C_m of approx. 1 μF/cm^2 for the swollen mitoplasts [1]. Accordingly, we do not purport that the dielectric permittivities in general differ by 3-fold between the outer and the inner membrane of rat liver mitochondria.

The equivalent permittivity for the inner compartment, ϵ_{ic}, of 50–60 is significantly smaller than ϵ_a and seems to be a likely estimate in the light of discussion in Paper I where we took into account the protein effect. The conductivity ratio κ_{ic}/κ_a of about 1/7 is not extremely out of proportion in view of the well preserved membranous substructures (Fig. 3) and the claimed presence of gel-like matrix [2] inside the intact mitochondria.

In conclusion, the dielectric dispersion technique coupled with a pertinent shell-model analysis has been demonstrated to provide a promising, non-invasive approach toward dissecting out the small vesicles' electrical parameters that are at present inaccessible by any other means.

Appendix

A theoretical model for the suspension of homogeneous double shells as shown in Fig. 1b is represented by the combination of text Eqns. 1, 3, 4 and 5. This model gave a compound dielectric dispersion which consisted essentially of two quasi-Debye type dispersions each having a characteristic frequency, f_{c1} or f_{c2}, and an associated permittivity increment, $\Delta\epsilon_1$ or $\Delta\epsilon_2$. Taking this into account we decided to divide the whole procedure into two steps. The first step was to fit the data of $\epsilon(f)$ to the following composite Debye type equation:

$$\epsilon(f) = \epsilon_h + \frac{\Delta\epsilon_1}{1 + (f/f_{c1})^2} + \frac{\Delta\epsilon_2}{1 + (f/f_{c2})^2} \tag{A1}$$

where $\Delta\epsilon_1 = \epsilon_1 - \epsilon_n$ and $\Delta\epsilon_2 = \epsilon_n - \epsilon_h$. Thus we have one set of phenomenological parameters (ϵ_1,

TABLE AI

RESPONSE OF PHENOMENOLOGICAL PARAMETERS TO INDIVIDUAL CHANGES (−50%) IN PHASE PARAMETERS

'Response' is expressed as % change from the starting value for a reference state defined by: $\epsilon_a = 80$, $\kappa_a = 10$ mS/cm, $\epsilon_{om} = 15$, $\epsilon_{im} = 10$, $\kappa_{om} = \kappa_{im} \leq 0.1$ μS/cm, $\epsilon_{oc} = 70$, $\kappa_{oc} = 8$ mS/cm, $\kappa_{ic} = 5$ mS/cm, $R = 0.5$ μm, $d_{om} = d_{im} = 7.0$ nm, $d_{oc} = 30$ nm, and $\phi = 0.3$.

Step in curve fitting	Phase parameter	% Change in phenomenological parameters				
		ϵ_l	ϵ_n	f_{c1}	f_{c2}	ϵ_h
1	ϵ_{om}	−46.7	−21.9	44.3	34.0	−1.5
2	ϵ_{im}	0.0	−33.6	22.9	53.0	−1.9
3	κ_{oc}	0.0	−1.1	−49.2	−2.8	0.2
4	κ_{ic}	0.0	5.5	−2.0	−42.9	1.0
5	ϵ_{ic}	0.0	0.0	0.0	4.3	−11.8
6	ϵ_{oc}	0.0	−0.2	0.2	0.2	−1.7

ϵ_n, ϵ_h, f_{c1} and f_{c2}) determined with a least-squares method.

The next step was to search for a set of electrical phase parameters so that these parameter values may reproduce as closely as possible the phenomenological parameters evaluated from the first step. To this end we calculated relative changes in the phenomenological parameters as functions of a 50% reduction in one of the phase parameters such as ϵ_{om}. The result is summarized in Table AI. The case for ϵ_{om}, presented on the top line of Table AI, implies that the phenomenological parameters other than ϵ_h are all sensitive functions of ϵ_{om}. In contrast, the parameter ϵ_{oc} is shown to be least effective in altering the general shape of the observable dispersion curves. Thus we now have a guideline along which to proceed in the curve fittings. Our strategy defined accordingly is as follows:

Step 0. Search and fix ϕ so that κ_l calculated may fit the observed κ_l.

Step 1. Search and fix ϵ_{om} so that ϵ_l calculated may fit the observed ϵ_l.

Step 2. Search and fix ϵ_{im} so that ϵ_n calculated may fit the observed ϵ_n.

Step 3. Search and fix κ_{oc} so that f_{c1} calculated may fit the observed f_{c1}.

Step 4. Search and fix κ_{ic} so that f_{c2} calculated may fit the observed f_{c2}.

Step 5. Search and fix ϵ_{ic} so that ϵ_h calculated may fit the observed ϵ_h.

Step 6. Repeat steps 1–5 for the best fit.

Acknowledgments

We wish to thank Mrs. T. Ichinowatari and Mr. K. Yagiu for their expert technical assistance. This work was supported in part by grants 548089, 56770052 and 56870020 from The Ministry of Education, Science and Culture, Japan.

References

1 Asami, K., Irimajiri, A., Hanai, T., Shiraishi, N. and Utsumi, K. (1984) Biochim. Biophys. Acta 778, 559–569
2 Lehninger, A.L. (1982) Principles of Biochemistry, Ch. 2, Worth Publishers, New York
3 Irimajiri, A., Doida, Y., Hanai, T. and Inouye, A. (1978) J. Membrane Biol. 38, 209–232
4 Irimajiri, A., Hanai, T. and Inouye, A. (1979) J. Theor. Biol. 78, 251–269
5 Maxwell, J.C. (1891) A Treatise on Electricity and Magnetism, 3rd Edn. Ch. 9, Clarendon Press, Oxford
6 Schwan, H.P. (1966) Biophysik 3, 181–201.
7 Cole, K.S. and Cole, R.H. (1941) J. Chem. Phys. 9, 341–351
8 Hanai, T., Koizumi, N. and Irimajiri, A. (1975) Biophys. Struct. Mech. 1, 285–294
9 Pauly, H. and Schwan, H.P. (1959) Z. Naturforsch. 14B, 125–131
10 Cole, K.S. (1970) in Physical Principles of Biological Membranes (Snell, F. et al., eds.), pp. 1–16, Gordon&Breach Science Publishers, New York